Preprint typeset in JINST style - HYPER VERSION

CALICE Analysis Note 008
May 21, 2008

Response of the CALICE Si-W ECAL Physics Prototype to Electrons

CALICE Collaboration

ABSTRACT: A prototype Silicon-Tungsten electromagnetic calorimeter for an ILC detector was installed and tested during summer and autumn 2006 at CERN. The detector had 6480 1x1 cm^2 silicon pads. Data were collected with electron and hadron beams in the energy range 1 to 50 GeV. The analysis described in this paper focuses on electromagnetic shower reconstruction and characterises the ECAL response to electrons in terms of energy resolution and linearity. The detector spatial uniformity and time stability are also addressed.

KEYWORDS: CALICE, ILC, electromagnetic calorimeter, silicon detector, electron reconstruction

.

Contents

1. Introduction

The CALICE collaboration is conducting R&D into calorimetric systems for the International Linear Collider (ILC) [1] — a proposed e^+e^- linear collider intended to operate in the centre of mass energy range up to 1 TeV. Interesting physics processes at the ILC include single or multiple Higgs boson production, pair production of top quarks, the formation of a spectrum of supersymmetric particles and the production of multiple gauge bosons. Such final states are typically characterised by multiple hadronic jets, accompanied in many cases by energetic leptons and/or missing energy.

The current designs of the calorimetry for detectors at the ILC are in large part driven by the demands of precise jet energy reconstruction. The target for the relative jet energy resolution is around $30\%/\sqrt{E/\mathrm{GeV}}$, which would permit W and Z bosons to be distinguished in their hadronic (two-jet) decay modes. With this level of performance, the precision with which their masses could be reconstructed would be comparable with their widths.

The target jet energy resolution is challenging, because it represents an improvement by a factor of two over the best obtained in previous detectors. One promising way to achieve it is through designing a detector system optimised for the so called "*particle flow*" approach, which relies on the reconstruction of as many particles in the jet as possible, using the suitable detector systems.

Thus, charged particles would be measured using the tracking system, photons (and possibly electrons) in the electromagnetic calorimeter, and neutral hadrons using the combined calorimetry. The success of such an algorithm depends on the quality of the pattern recognition in the calorimeters. In designing a calorimetric system optimised for particle flow, a high spatial granularity is therefore more important than the intrinsic energy resolution for single particles. Furthermore, the overall design of the detector (tracking, electromagnetic and hadronic calorimetry) needs to be considered in a coherent way.

The design of the ILC detectors can be optimised by Monte Carlo simulation, but in order to do this, it is crucial to validate the Monte Carlo tools with data. Therefore, the R&D of the CALICE collaboration has two broad aims. The first is to construct realistic calorimeter prototypes, and learn about their operation and behaviour in beam tests. The second objective is to confront the data with Monte Carlo simulations using the same tools used for the full detector. This is especially important in the case of hadronic showers, where many models are available, which make differing predictions for the calorimeter response. The CALICE plan is to expose complete calorimeter systems (electromagnetic and hadronic, using various technologies) to test beams of electrons, muons and hadrons. To this end, a first round of beam tests was performed at DESY and CERN in summer 2006, using a Silicon-Tungsten sampling electromagnetic calorimeter [2], followed by a hadron calorimeter composed of iron and scintillator tiles [3], and then a "tail catcher" of iron instrumented with scintillator strips [4].

In this paper, we report results of exposition of the electromagnetic calorimeter (ECAL) to electron and positron beams in the energy range 6-50 GeV at the CERN SPS beam line [5]. In Section 2 we outline the arrangement in the test beams. The ECAL is briefly described in Section 3 and some key technical aspects of its performance highlighted. Section 4 summarises the Monte Carlo simulation. Features of the electron beam data are over-viewed in Section 5 and the uniformity across the detector is addressed. The results of the energy measurement together with some of their systematic uncertainties are presented in Section 6 for the detector areas of uniform response.

2. Experimental Setup

A sketch of the CERN H6 [5] test beam setup is presented in Figure 1 and a detailed description of the detectors can be found in [2]. The physics program and the overall collected electron, pion and muon statistics are extensively discussed in the same reference. The beam trigger was defined by the coincidence signal of three scintillator counters. In addition, four drift chambers were used to monitor the beam. Čerenkov detectors were also available for e/π discrimination.

The calorimeter response to electrons is measured in this paper for electron tracks normally incident on ECAL. The event display for one of these events is shown in Figure 2.

3. The ECAL prototype

A detailed description of the ECAL hardware is given in [2], along with details of the commissioning and a number of technical features of the system calibration and performance. The ECAL prototype consisted of 30 layers of tungsten, the first ten of thickness 1.4 mm, the next ten of 2.8 mm,

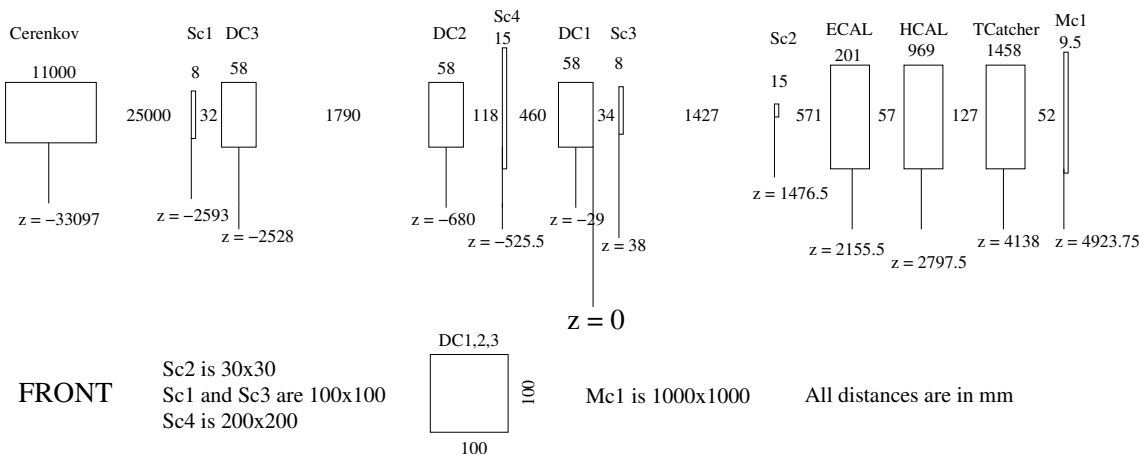

Figure 1. Sketch of the CERN test beam setup. The right handed coordinate system used hereafter is indicated: the backside of the drift chamber closer to ECAL (DC1) defines the $z = 0$ plane.

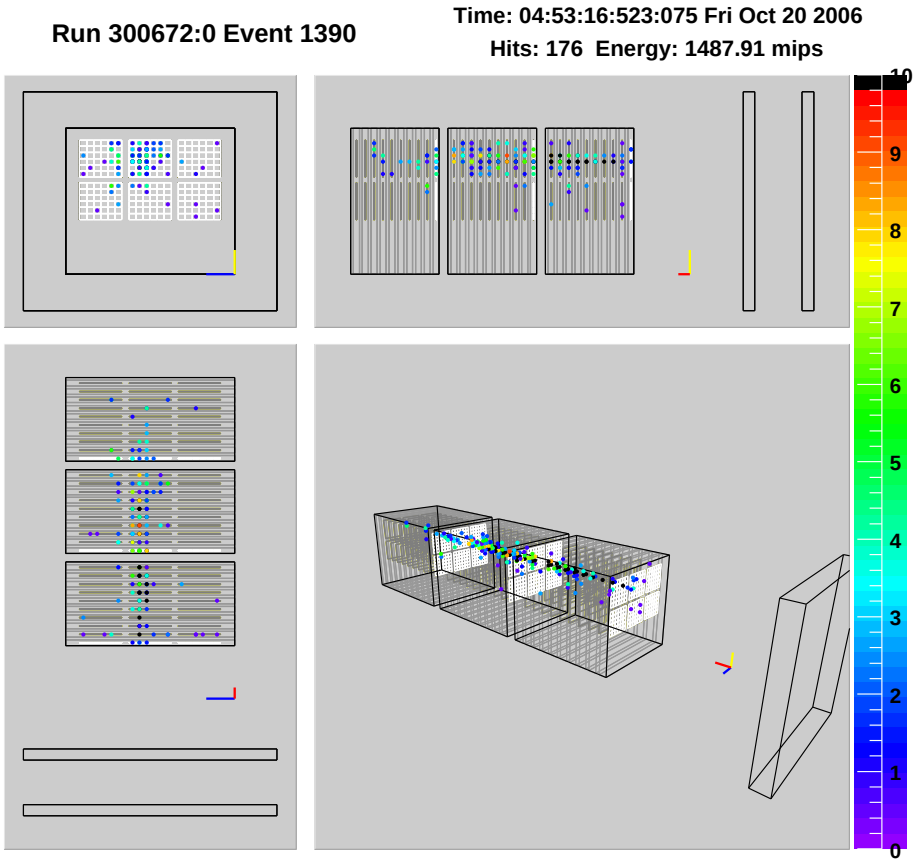

Figure 2. A typical 10 GeV e^- shower in ECAL. The detector cells with signal above 0.5 MIPs threshold are displayed with the colour scale shown on the right. Layout not to scale.

and the last ten of 4.2 mm, comprising 24 radiation lengths in total at normal incidence. The development of the showers was sampled using 30 layers of silicon PIN diode pads interleaved between

the tungsten plates. The silicon thickness was 525 μm, and each pad had dimensions 1×1 cm^2. The sensors were made on 4 inch wafers in units of 6×6 pads. At the time of the 2006 CERN beam tests, each layer consisted of a 3×2 array of wafers, *i.e.* 18 pads horizontally and 12 pads vertically, leading to a total of 6480 pads for the ECAL. Around the pads in each wafer, a non-active region of 1.8 mm width was used for a grounded guard ring structure.

Blocks of random triggers were recorded during data taking in order to monitor pedestals and noise. Short term changes and shifts in pedestals caused by large signals in neighbouring cells were monitored and corrected using cells without signal in beam events [2]. The uncertainty on the pedestal levels was estimated to be less than 0.2% of the signal associated with a minimum ionising particle (MIP), negligible compared to the energy deposited by a typical electron shower. The noise level was typically 0.13 MIPs. Its spread channel-to-channel was 9% of the mean noise and the spread run-to-run was less than 1% of the mean noise. The low spread of the noise motivated a hit energy threshold unique for the whole detector.

Calibration constants for each pad were determined using muon events. The response of each cell was fitted by a convolution of a Landau distribution with a Gaussian. The most probable value of the underlying Landau function was taken to define the MIP value for each cell, and the raw energy for each cell in data was corrected to units of MIPs. All but 9 pads were functioning and successfully calibrated. The calibration constants were determined with an accuracy of 0.5% and had a cell to cell dispersion of 5%. Data taken in the various beam test periods during summer and autumn 2006 held well correlated calibration constants, with differences less than 1.6%.

One feature of the data which has not been corrected is associated with showers which deposit a sizable energy in the guard ring surrounding a wafer. This is a cause of correlated crosstalk, observed as a distinctive square pattern of low energy hits in a number of cells around the periphery of the wafer. The prevalence of this effect increases with shower energy. In the future, the design of the guard rings will be modified in order to prevent this problem.

After calibration, the ECAL data consist of hits in the cells of the calorimeter with energies in units of MIPs. In order to remove most of the noise signals, a threshold cut of 0.6 MIP was imposed on each cell, almost five times the mean noise level.

4. Monte Carlo Simulation

The test beam setup is simulated with Mokka [6], a Geant4 [7]-based Monte Carlo program, followed by a digitisation module simulating the response of the data acquisition electronics. All material in front of the ECAL is accounted for to the best of our knowledge. The subdetectors are simulated with different levels of detail, depending on their impact on the physics analysis: material simulation only for the Čerenkov detectors, Geant4 hits for the trigger, partial electronics simulation for the tracking detectors, full simulation up to the digitisation level, with a detailed electronics simulation, for the ECAL.

The beam simulation assumes a parallel beam with Gaussian width reproducing the observed beam profile. To study systematic effects due to shower lateral leakage, samples are also generated with a beam uniform over the ECAL front face. A Gaussian momentum dispersion consistent with the settings of the beam collimators [5] is applied for each run.

5. Selection of Electron Events

The selection of single electron showers from data relies on the energy recorded in the ECAL. This energy, E_{raw}, is calculated with the three ECAL stacks weighted in proportion to the tungsten thickness:

$$E_{\mathrm{raw}} = \sum_{i=0}^{i=9} E_i + 2\sum_{i=10}^{i=19} E_i + 3\sum_{i=20}^{i=29} E_i, \tag{5.1}$$

where E_i is the energy deposit in layer i. The distribution of E_{raw} is shown in Figure 3 for a typical 20 GeV run. The electron peak around 5000 MIPs is clearly visible; however, the beam contamination with muons or pions gives an additional peak at 50 MIPs and the region between the two main peaks is populated with pions. Electron candidates are selected by requiring:

$$125 < \frac{E_{\mathrm{raw}}(\mathrm{MIP})}{E_{\mathrm{beam}}(\mathrm{GeV})} < 375.$$

The significant pion contamination present in some of the runs is reduced by demanding a trigger signal from the threshold Čerenkov counter in the beam. The effect of this additional selection is indicated by the shaded region in Figure 3.

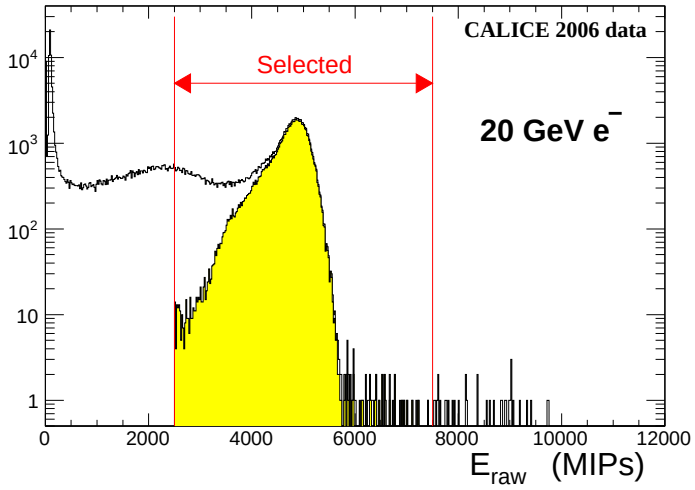

Figure 3. *Distribution of total ECAL hit energies for a 20 GeV beam. The E_{raw} selection window and the shaded area obtained by demanding a signal from the Čerenkov counter are shown.*

5.1 Rejection of the beam halo

The rejection of the beam halo is implemented on a run by run basis. The x and y acceptance for the incoming electron track is chosen such as to achieve a reasonably flat distribution of the mean energy deposition in the ECAL.

5.2 Inter-wafer gap effect

The inter-wafer gaps of 1.8 mm due to the guard rings have an influence on the response when showers traverse these regions of the calorimeter. This is illustrated in Figure 4 for 30 GeV e^-

impinging on the calorimeter at normal incidence. Here the mean value of E_{raw}(Eq. 5.1) is plotted as a function of the shower barycentre $(\bar{x},\bar{y})$, defined as :

$$(\bar{x},\bar{y}) = \sum_i (E_i x_i, E_i y_i) / \sum_i E_i$$

The sums run over all hit cells in the calorimeter. Dips in response corresponding to the guard ring positions are clearly visible. According to Figure 6, which shows the mean value of E_{raw} as a function of the shower barycentre for 20 GeV electrons, the energy loss is about 15 % when tracks impinge in the centre of the x gaps and about 20 % in the case of the y gap.

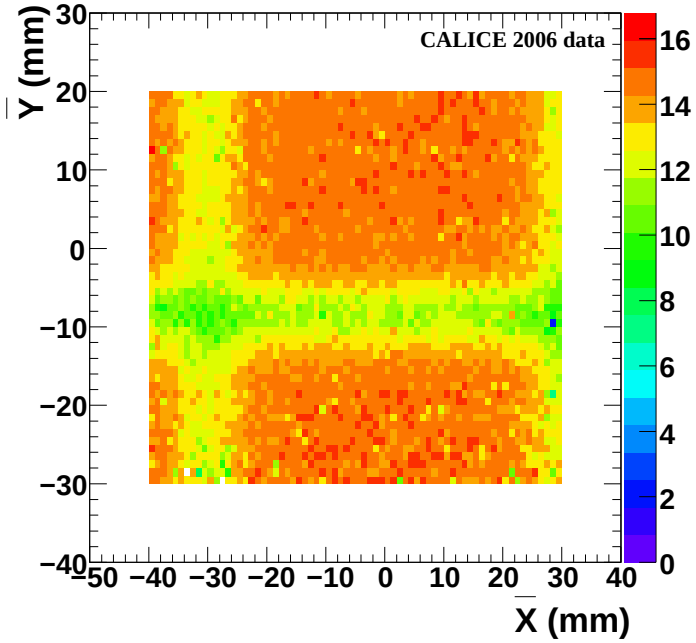

Figure 4. *Mean values of E_{raw} for a 15 GeV e^- beam as function of the barycentre coordinates.*

In order to recover this loss and to have a more uniform calorimeter response, a simple method was investigated. The ECAL energy response, $f(\bar{x},\bar{y}) = E_{\mathrm{raw}}/E_{\mathrm{beam}}$, is measured using a combined sample of 10, 15 and 20 GeV electrons, equally populated and the energy of each shower is corrected by $1/f$.

The response function f is displayed on Figure 5. It can be parameterised with Gaussian functions, independently in $\bar{x}$ and $\bar{y}$:

$$f(\bar{x},\bar{y}) = \left(1 - a_x e^{-\frac{(\bar{x}-x_{gap})^2}{2\sigma_x^2}}\right)\left(1 - a_y e^{-\frac{(\bar{y}-y_{gap})^2}{2\sigma_y^2}}\right)$$

The results of the Gaussian parametrisations are given in Table 1. The gap in x is shallower and wider than that in y, due to the staggering of the gaps in x [2].

As illustrated in Figure 6, when the gap corrections are applied, the energy loss in the gaps is reduced to a few percent level. The low energy tail in the energy distribution is also much reduced

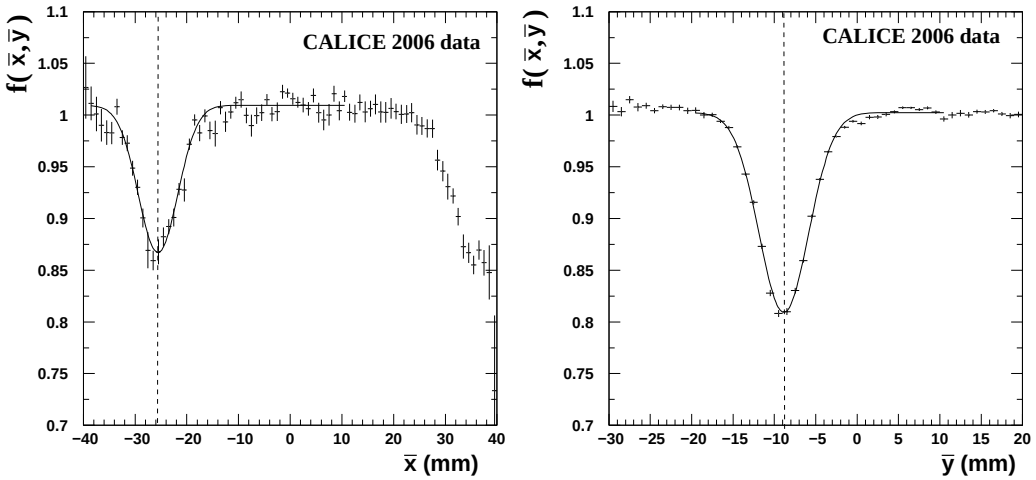

Figure 5. *$f(\bar{x},\bar{y})$ function of the shower barycentre coordinates, for a combined sample of 10, 15 and 20 GeV electrons. To characterise the x (y) response, the events were requested to be outside the inter-wafer gap in y (x), leading to an important difference in the number of events for the two distributions, since the beam is centred on the y gap.*

	position (mm)	σ (mm)	a
x direction	-30.01	4.3	0.143
y direction	-8.4	3.19	0.198

Table 1. Gaussian parametrisation of the inter-wafer gaps.

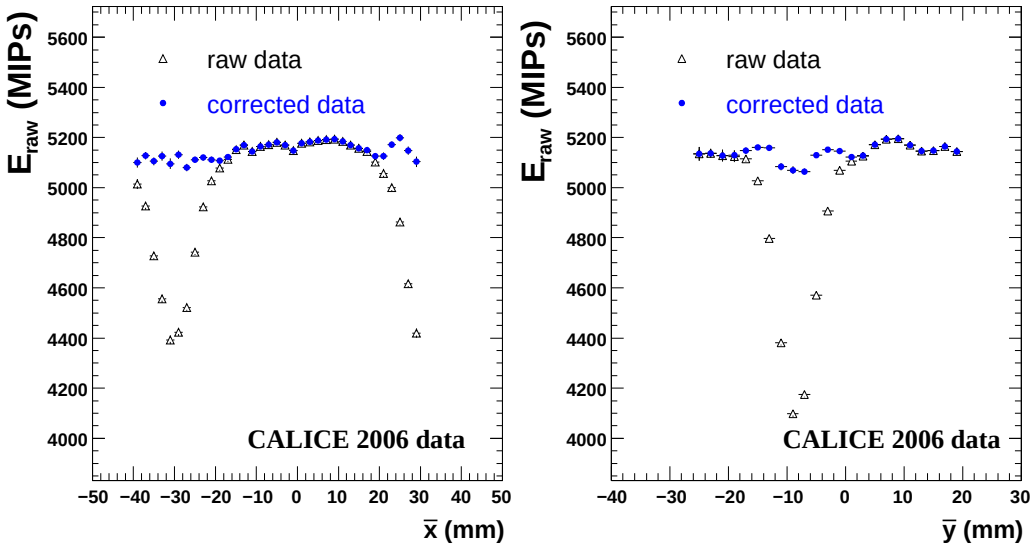

Figure 6. Mean E_{raw} function of the shower barycentre coordinates for 20 GeV electrons, before (black triangles) and after the corrections (blue circles) were applied on E_{raw}.

(Figure 7). The correction method relies only on calorimetric information and can be applied both for photons and electrons.

Even if it is possible to correct, statistically, for the interwafer gaps, per event their presence

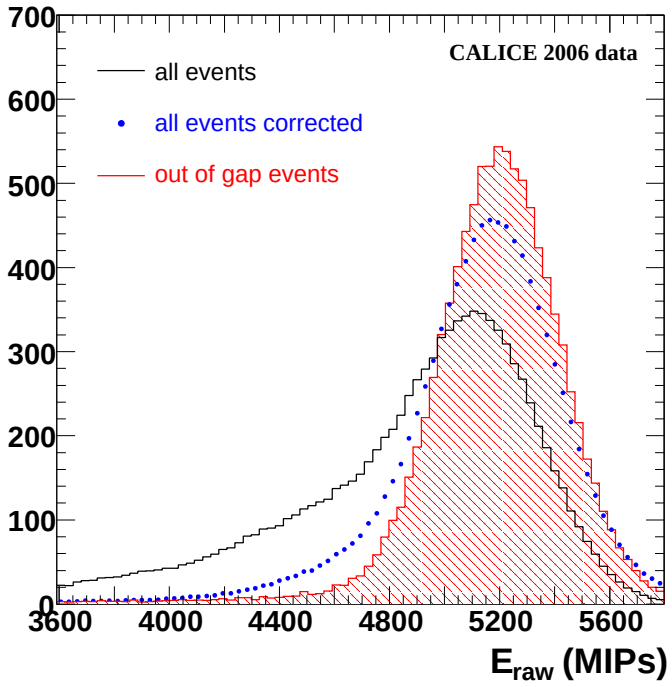

Figure 7. Energy distribution for 20 GeV electrons in case of: events outside the inter-wafer gaps (red histogram), all events without corrections (black histogram) and all events with corrections (blue circles). The histograms are normalised to the same number of entries, for an easier comparison.

will induce fluctuations in the energy response and deteriorate the ECAL resolution compared to a continuous calorimeter. It is however difficult to estimate their effect, since it depends strongly on the beam profile, which was relatively narrow and with a width varying with the beam energy.

For this analysis, only particles impinging in the middle of the wafers are selected in order to reduce the impact of the beam profile on the characterisation of the ECAL prototype performance. Since the gap effect is considered to be negligible more than 4σs away from the gap centre, the position of the shower barycentre for selected events is required to be farther than 17.2 mm (12.76 mm) from the inter-wafer gap position along x (y).

5.3 Selection of showers well contained in ECAL

The fiducial volume in which the showers are fully contained in the ECAL was estimated using electron tracks away from the inter-wafer gaps and pointing to the centre of the ECAL. The radial shape of an average 20 GeV electron shower is shown in Figure 8. More than 97% of the shower energy is contained within 4 cm (*i.e.* four pads). All electrons wherethe impact point of the track on the ECAL front face lay less than 4 cm from one of the ECAL borders are excluded from the selected sample.

A summary of the selected electron and positron data is shown in Table 2.

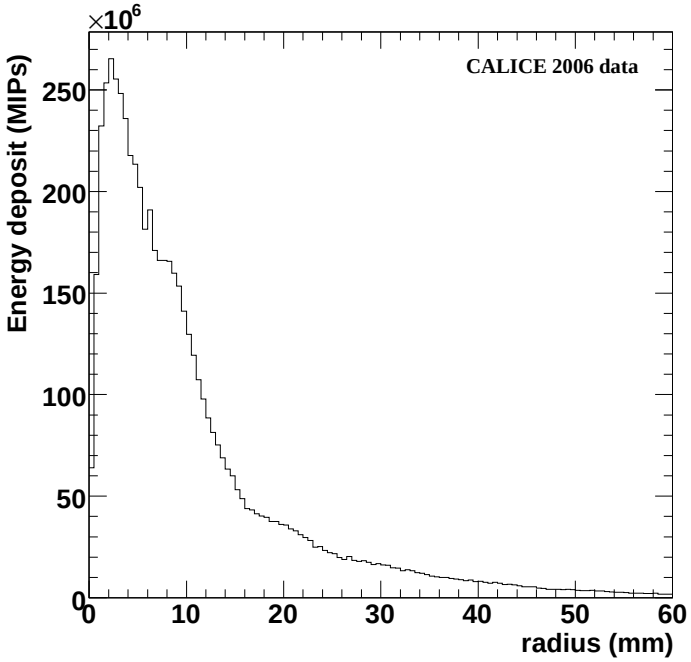

Figure 8. *Energy deposited in ECAL as function of the radial distance to the shower axis, for an average 45 GeV shower.*

Energy (GeV)	particle	date	statistics (kevts)
6	e^-, e^+	Oct	10.6
10	e^-, e^+	Aug, Oct	55.9
12	e^-, e^+	Oct	32.1
15	e^-, e^+	Aug, Oct	60.4
20	e^-, e^+	Aug, Oct	76.9
30	e^-, e^+	Aug, Oct	43
40	e^-	Aug	27
45	e^-	Aug	129.3

Table 2. *Summary of the electron events selected for this analysis.*

6. Performance Studies

6.1 ECAL Sampling Fraction Scheme

The ECAL is made of 30 layers grouped in three stacks of 10 layers each [2]. Each tungsten sheet has the same thickness in a given stack. However, due to the mechanical structure of the ECAL slabs, two successive silicon layers are either separated by one thickness of tungsten or by the same thickness of tungsten plus two thicknesses of PCB, aluminium and carbon-fibre–epoxy composite, as shown in Figure 9. A different sampling fraction, defined as the ratio of the energy deposited in the active medium to the total energy deposit (sum of the energy deposits in the active *and* passive medium), is therefore expected for the even and the odd layers of the same calorimeter stack.

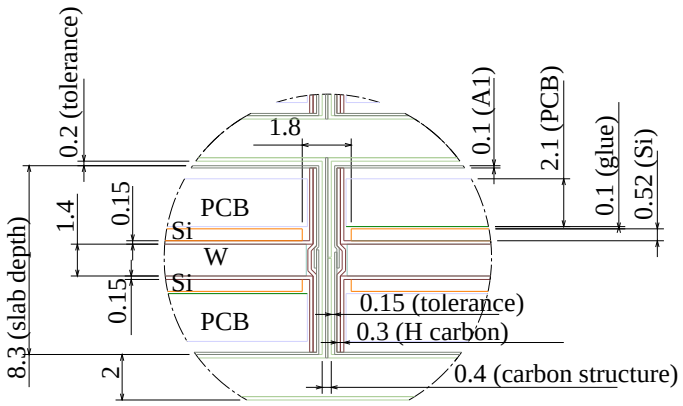

Figure 9. *Details of one ECAL slab, showing one passive tungsten layer sandwiched between two active silicon layers. The lower silicon layer is preceded by a larger passive layer compared to the upper one: the PCB, aluminium , glue, etc add to the tungsten.*

The easiest method to investigate this difference is to compare in each stack the mean energy deposits in odd and even layers. For the first stack, if we neglect the shower profile, the ratio of the two is

$$R = \frac{E^{\text{odd}}}{E^{\text{even}}} = 1 + \eta,$$

with η being, approximately, the ratio of the non-tungsten radiation length to the tungsten radiation length.

When counting the layers starting from zero, the odd layers are systematically shifted compared to the even layers towards the shower maximum and the measurement of R is biased by the shower development. To overcome this bias, R is measured twice, either comparing the odd layers with the average of the surrounding even layers, or comparing the even layers with the average of the neighbouring odd layers:

$$R' = \frac{\langle \mathrm{E}_1 + \mathrm{E}_3 + \mathrm{E}_5 + \mathrm{E}_7 \rangle}{\left\langle \frac{\mathrm{E}_0+\mathrm{E}_2}{2} + \frac{\mathrm{E}_2+\mathrm{E}_4}{2} + \frac{\mathrm{E}_4+\mathrm{E}_6}{2} + \frac{\mathrm{E}_6+\mathrm{E}_8}{2} \right\rangle}$$

$$R'' = \frac{\left\langle \frac{\mathrm{E}_1+\mathrm{E}_3}{2} + \frac{\mathrm{E}_3+\mathrm{E}_5}{2} + \frac{\mathrm{E}_5+\mathrm{E}_7}{2} + \frac{\mathrm{E}_7+\mathrm{E}_9}{2} \right\rangle}{\langle \mathrm{E}_2 + \mathrm{E}_4 + \mathrm{E}_6 + \mathrm{E}_8 \rangle}$$

where E_n is the energy deposit in the layer number n and the brackets indicate that mean values are used. The value of η is taken as the average of $R' - 1$ and $R'' - 1$, whereas the difference between them gives a conservative estimate of the systematic error due to the shower shape. As an example, the distribution of the energy deposits in the odd and even layers is shown in Figure 10 for 20 GeV electrons.

The overall value of η is $7.2 \pm 0.2 \pm 1.7\%$, while the individual values of η, obtained for each beam energy, are displayed in Figure 11. The measurement of η using the second and third stack, as well as simulated data, leads to compatible results.

In computing the total response of the calorimeter, the sampling fraction for layer i is given by $w_i = K = 1,\ 2,\ 3$ for even layers in stacks 1, 2, 3 and $w_i = K + \eta$ for the odd layers, respectively.

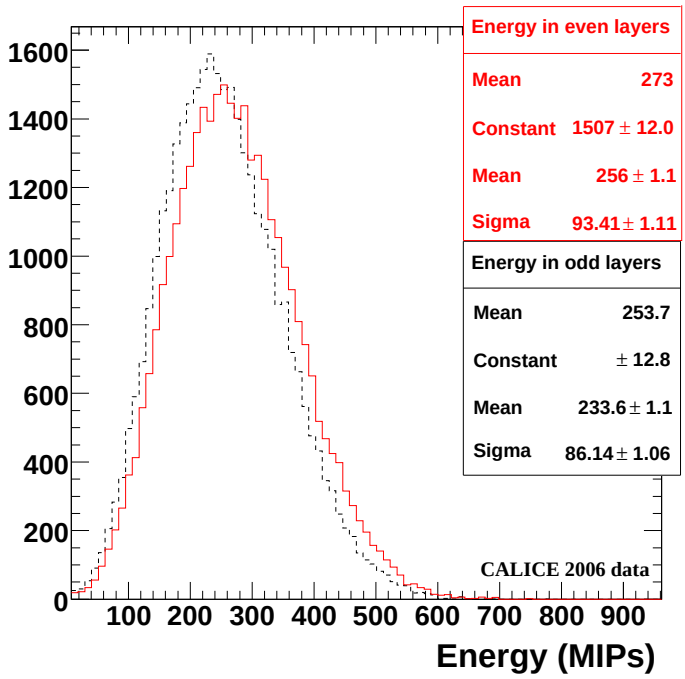

Figure 10. *Energy deposits in odd end even layers by 20 GeV electrons. The statistical information corresponds to Gaussian parametrisations of the two distributions.*

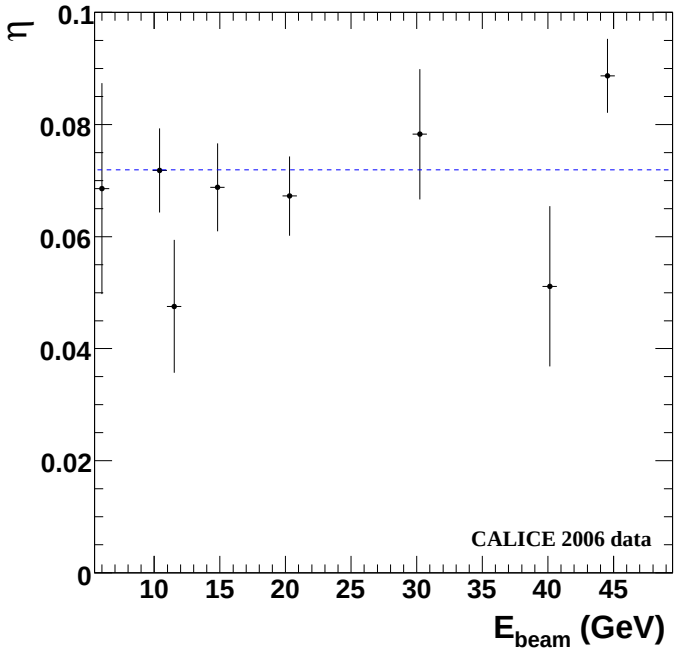

Figure 11. η *as function of the beam energy.*

6.2 Linearity and energy resolution

The total response of the calorimeter is calculated as

$$E_{\mathrm{rec}}(\mathrm{MIPs}) = \sum_i w_i E_i$$

with w_i the sampling fraction for the layer i. Its distribution for electrons at 30 GeV is shown in Figure 12, together with a fit using a Gaussian function in the range $[-\sigma,+2\sigma]$. An asymmetric range is chosen in order to reduce sensitivity to pion background, to radiative effects upstream of the calorimeter, and to any residual influence of the inter-wafer gaps. The position of the peak is the mean energy response (E_{mean}) and its distribution is shown in Figure 13 as function of the beam energy. The errors on E_{mean} are those estimated from the fit.

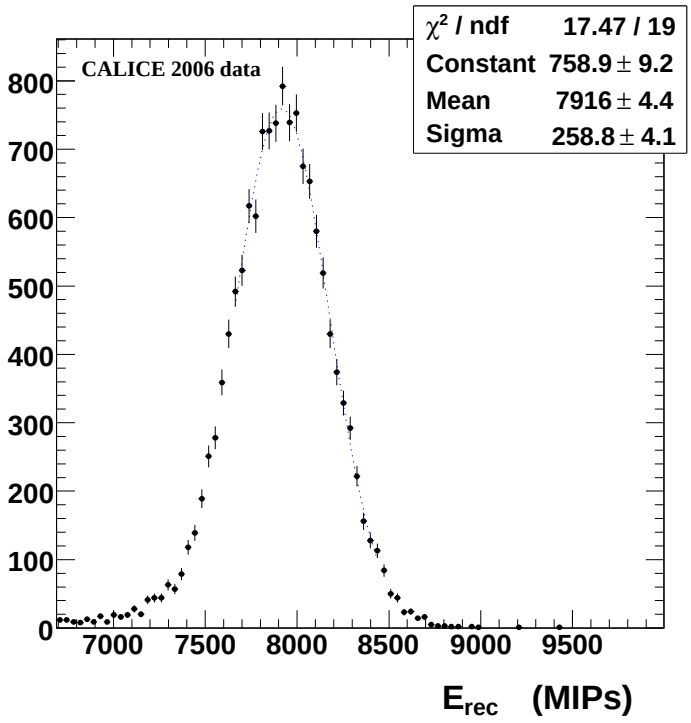

Figure 12. *Gaussian parametrisation of E_{rec} for a 30 GeV electron run. The range of the fit is $[-\sigma,+2\sigma]$.*

From the dispersion of E_{rec} in the different runs at the same nominal beam energy, the error of the beam mean energy, E_{beam}, was estimated to be

$$\frac{\Delta E_{\text{beam}}}{E_{\text{beam}}} = \frac{0.12}{E_{\text{beam}}(\text{GeV})} \oplus 0.1\%, \tag{6.1}$$

The first term is related to hysteresis in the bending magnets, while the calibration and the uncertainties on the collimator geometry give the constant term.

The mean energy response can be parametrised as $E_{\text{mean}} = \beta \cdot E_{\text{beam}} - \alpha$, while the *measured* energy E_{meas} is given by $E_{\text{meas}} = E_{\text{mean}} + \alpha$. The parameter β is a global MIP to GeV calibration factor. The offset α is partly due to the rejection of the low energy hits and it increases steadily with the hit energy threshold, as displayed on Figure 14.

The residuals to linearity of the measured energy are shown in Figure 15 as function of the beam energy. The non-linearities are at the percent level.

The relative energy resolution, $\Delta E_{\text{meas}}/E_{\text{meas}}$, as shown in Figure 16, can be parametrised by

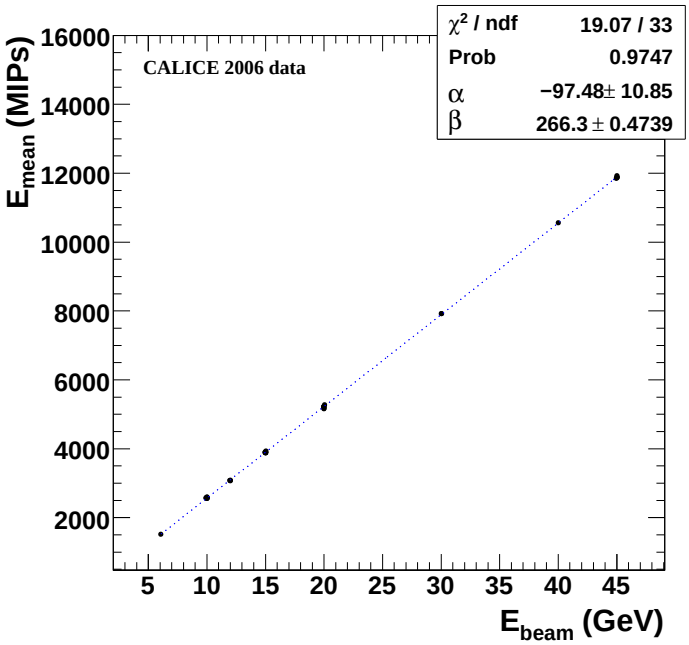

Figure 13. *Energy response of the ECAL function of the beam energy.*

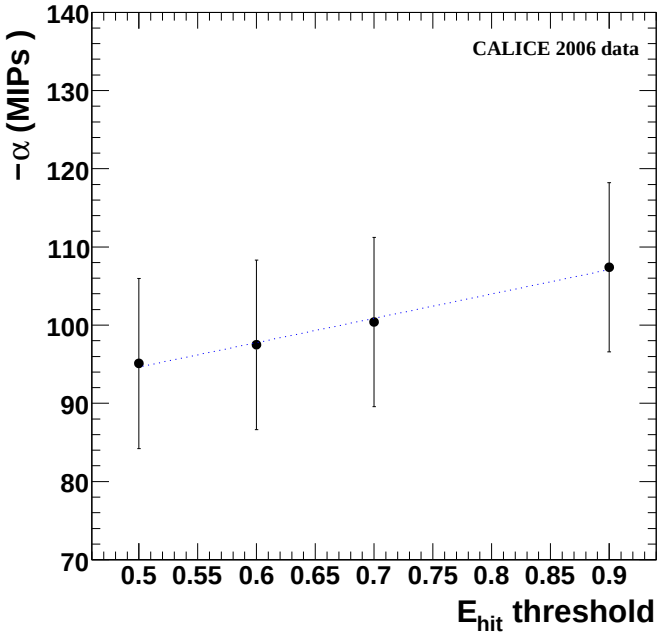

Figure 14. *Variation of the linearity offset with the hit energy threshold.*

a quadrature sum of stochastic and constant terms

$$\frac{\Delta E_{\text{meas}}}{E_{\text{meas}}} = \frac{16.69 \pm 0.13}{\sqrt{E\,(\text{GeV})}} \oplus (1.09 \pm 0.06)\,\% \,,$$

where the intrinsic momentum spread of the beam was subtracted from the ECAL data [5].

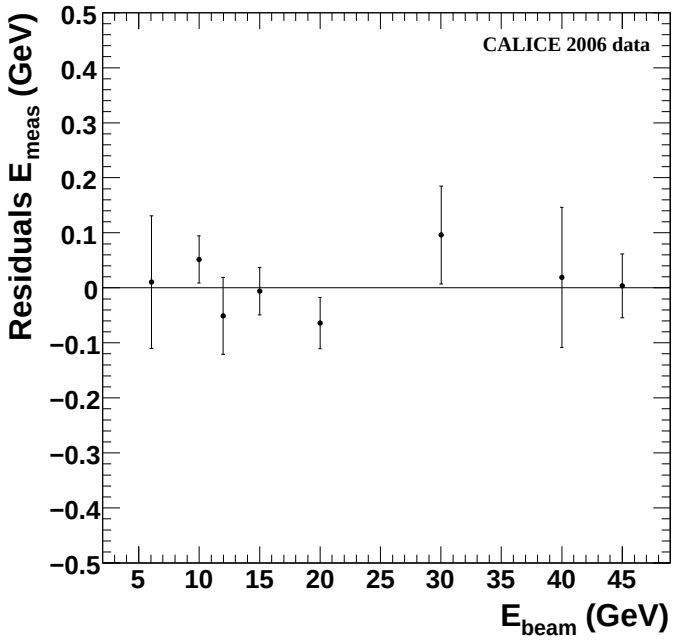

Figure 15. *Residuals to linearity of E_{meas} function of the beam energy. All the runs around the same nominal energy of the beam were combined in one entry, for which the uncertainty was estimated assuming that the uncertainties on the individual runs were uncorrelated.*

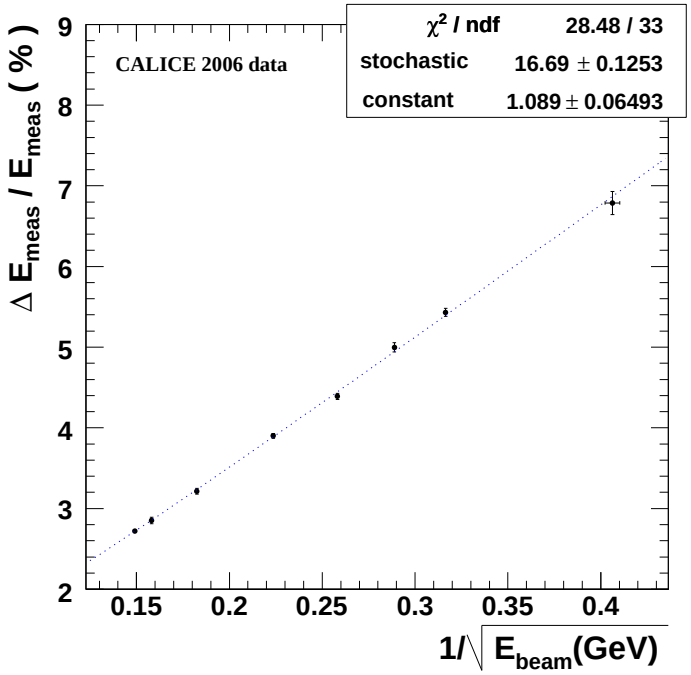

Figure 16. *Relative energy resolution ($\Delta E / E_{\mathrm{meas}}$) function of the beam energy. For clarity sake, the 35 runs available were combined into 8 different beam energy points for the plot. For the parametrisation of the energy resolution each run was however treated individually.*

Different systematic checks have been performed on the data. Variations of the linearity and resolution against the minimal accepted distance between the shower barycentre and the nearest inter-wafer gap, when the energy threshold for considering the hits is 0.5 MIPs are shown in Table 3. In addition, this hit energy threshold has been itself varied (Table 4). In order to investigate the potential effects linked to the beam position, the energy response is also compared for showers with barycentres located in the right hand side and in the upper half of the detector (Table 5), respectively. The results are consistent. Since data were taken in both August and October 2006, it was also possible to check the response stability in time and no significant differences between the two data samples are observed.

	shower distance to the gaps (in nb of σs)			
	3.5	4	4.5	5
χ^2/ndf (linearity)	18.4/33	19.7/33	19.8/33	24.1/32
α (MIPs)	-91.7$\pm$10.8	-95.1$\pm$10.9	-97.9$\pm$11.2	-100.8$\pm$11.4
β (MIPs/GeV)	266.2$\pm$0.5	266.6$\pm$0.5	266.8$\pm$0.5	267$\pm$0.5
resol (stat term)	17$\pm$0.1	16.9$\pm$0.1	16.8$\pm$0.2	16.7$\pm$0.2
resol (ct term)	1$\pm$0.1	1$\pm$0.1	1$\pm$0.1	1$\pm$0.1

Table 3. *Impact of the distance of shower to the inter-wafer gaps on the ECAL linearity and resolution. The distance is given in terms of σs to the gap centre, with σ defined by the Gaussian parametrisation of the gaps. The beam momentum spread is not subtracted from the data. The hit energies are required to be larger than 0.5 MIPs.*

7. Conclusion

The response to normally incident electrons of the Calice Si-W electromagnetic calorimeter was measured for energies between 6 and 45 GeV, using the data recorded during 2006 testbeam at CERN.

The calorimeter is linear to 1% level. The energy resolution has a stochastic term of 16.69$\pm$0.13, whereas the constant term is 1.09$\pm$0.06.

A simple method of correcting for non-uniformities in the calorimeter response due to non active regions between the silicon wafers was found. It allows to recover, statistically, most of the lost energy.

References

[1] T. Behnke *et al* (ed.), Reference Design Report "Volume 4: Detectors", available at `http://lcdev.kek.jp/RDR`

	E_{hit} cutoff (MIPs)		
	0.6	0.7	0.9
χ^2/ndf (linearity)	19.1/33	18.9/33	20.1/33
α (MIPs)	-97.5 $\pm$10.9	-100.4$\pm$10.8	-107.4$\pm$10.8
β (MIPs/GeV)	266.3$\pm$0.5	266.1$\pm$0.5	265.5$\pm$0.5
resol (stat term)	16.8$\pm$0.1	16.8$\pm$0.1	16.9$\pm$0.1
resol (ct term)	1.1$\pm$0.1	1.1$\pm$0.1	1$\pm$0.1

Table 4. *Impact of the hit energy cutoff on the ECAL linearity and resolution. The beam momentum spread is not subtracted from the data.*

	right side	upper part
α (MIPs)	-96.1$\pm$10.9	-97.7$\pm$11
β (MIPs/GeV)	266.6$\pm$0.5	266.8$\pm$0.5
resol (stat term)	16.8$\pm$0.1	16.8$\pm$0.2
resol (ct term)	1.1$\pm$0.1	1.1$\pm$0.1

Table 5. *Response to electrons crossing the right hand side and, respectively, the upper part of ECAL. The beam momentum spread was not subtracted from these data.*

[2] J. Repond *et al*, "Design and Commissioning of the Physics Prototype of a Si-W Electromagnetic Calorimeter for the International Linear Collider", to be submitted to JINST.

[3] F. Sefkow, "The scintillator HCAL testbeam prototype", in the Proceedings of 2005 International Linear Collider Workshop (LCWS 2005), Stanford, California, March 2005.

[4] D. Chakraborty, "The Tail-Catcher/Muon Tracker for the CALICE Test Beam"', in the Proceedings of 2005 International Linear Collider Workshop (LCWS 2005), Standford, California, March 2005.

[5] Description of the CERN H6 testbeam area available at `http://ab-div-atb-ea.web.cern.ch/ab-div-atb-ea/BeamsAndAreas/`

[6] "Mokka Geant4 Application for Linear Collider Detectors", see `http://polzope.in2p3.fr:8081/MOKKA.`

[7] S. Agostinelli *et al*, "Geant4 — A Simulation Toolkit", NIM A 506 (2003) 250-303.